Journal of The Korean Astronomical Society
46: 65 ∼ 74, 2013 April

http://dx.doi.org/10.5303/JKAS.2013.46.2.65
ISSN:1225-4614
http://jkas.kas.org

HOW TO MONITOR AGN INTRA-DAY VARIABILITY AT 230 GHZ

Jae-Young Kim[1] and Sascha Trippe[1]
[1]Department of Physics and Astronomy, Seoul National University, Seoul 151-742, Korea
E-mail : dadu1543@snu.ac.kr, trippe@astro.snu.ac.kr
(Received December 21, 2012; Revised February 4, 2013; Accepted February 5, 2013)

ABSTRACT

We probe the feasibility of high-frequency radio observations of very rapid flux variations in compact active galactic nuclei (AGN). Our study assumes observations at 230 GHz with a small 6-meter class observatory, using the SNU Radio Astronomical Observatory (SRAO) as an example. We find that 33 radio-bright sources are observable with signal-to-noise ratios larger than ten. We derive statistical detection limits via exhaustive Monte Carlo simulations assuming (a) periodic, and (b) episodic flaring flux variations on time-scales as small as tens of minutes. We conclude that a wide range of flux variations is observable. This makes high-frequency radio observations – even with small observatories – a powerful probe of AGN intra-day variability; especially, those which complement observations at lower radio frequencies with larger observatories like the Korean VLBI Network (KVN).

Key words : Galaxies: active — Radiation mechanisms: non-thermal — Methods: statistical

1. INTRODUCTION

Active galactic nuclei (AGN; for a review, see e.g., Beckmann & Shrader 2012) show strong flux variations on various timescales. On the shortest timescales, intra-day variability (IDV) of radio fluxes was first reported by Witzel et al. (1986). Since then, such rapid variability has been observed throughout the electromagnetic spectrum mainly in compact objects, such as flat spectrum radio quasars (FSRQs) and BL Lacertae objects (BL Lacs). At frequencies around 5 GHz, about half of all FSRQs have been reported to show IDV (Lovell et al. 2008).

A priori, such rapid variability is hard to understand. For a given observed variability time scale $t_{\rm var}$ the spatial extension of the emission region is limited to $c\,t_{\rm var}/(z+1)$, with c denoting the speed of light and z being the redshift. The observed brightness temperature is related to the variability time scale as follows: $T_b \propto [t_{\rm var}\,(z+1)]^{-2}$; observed values are as high as $T_b \approx 10^{18}$ K (Wagner & Witzel 1995; Fuhrmann et al. 2008). However, cooling by inverse Compton scattering limits the brightness temperature of realistic plasmas to $T_b \lesssim 10^{12}$ K (Kellermann & Pauliny-Toth 1969) – in apparent contradiction to observations.

In order to understand intra-day variability, several intrinsic and extrinsic origins of IDV have been proposed. The most important *extrinsic* mechanism is *interstellar scintillation* (ISS): turbulent motion of ionized interstellar matter focuses and de-focuses the light from AGN on its way to Earth. ISS has been identified observationally by annual modulations of IDV caused by the motion of the Earth around the sun (Gabanyi et al. 2007; Liu et al. 2012; Marchili et al. 2012). However, the amplitude of interstellar scintillation scales with the observation frequency ν as $\nu^{-2.2}$ (Rickett, Coles & Bourgois 1984). Accordingly, the contribution by ISS to AGN variability is substantial at cm-radio frequencies but increasingly unimportant at mm-radio and shorter wavelengths. In addition, the observed correlation between rapid variability in radio and optical wavelength regimes indicates intrinsic causes (Wagner & Witzel 1995).

The most important *intrinsic* mechanism for intra-day variability is a combination of rapid intrinsic variability of the source – especially shocks in AGN jets (Blandford & Königl 1979) – plus Doppler boosting. In order to reconcile the observed brightness temperatures with the inverse Compton limit, Doppler factors of the order of 10 to 100 are necessary – which are high, yet realistic values (Fuhrmann et al. 2008).

An analysis of plasma-physical processes related to AGN outflows usually requires radio observations as the emission from AGN jets is – essentially – synchrotron radiation; the flux density F_ν approximately follows a power law $F_\nu \propto \nu^{-\alpha}$ with $\alpha \approx 0$–1. Addressing intra-day variability requires flux monitoring observations that (1) operate at high frequencies $\nu \gtrsim 100$ GHz in order to bypass ISS, (2) have good ($\lesssim$1 h) time resolution, (3) cover observing times as long as possible in order to allow for detailed time-series analysis, and (4) provide a decent signal-to-noise ratio in order to detect even small ($\lesssim$10%) variations. Evidently, these criteria are somewhat in conflict for realistic observations: on the hand, criteria 2 and 4 suggest the use of large radio observatories; criterion

Corresponding Author: S. Trippe

Table 1.
Parameter values and corresponding noise levels

Parameter	Value
A_e/A_0	0.55
Δt	100 s
$\Delta\nu$	1 GHz
T_{rec}	55 K
T_{atm}	263 K
T_{amb}	273 K
τ_0	1.5
η	0.9
ρ_A	180 Jy K^{-1}
T_{sys}	290 K
δT	0.92 mK
σ_N	0.16 Jy

3 suggests the exclusive use of a given observatory for long periods, potentially many days. Accordingly, the scheduling of such programs has been notoriously difficult (cf. e.g., Fuhrmann et al. 2008).

Our work explores an approach complementary to observations at large observatories. We analyze the performance achievable by using a small, 6-meter class, radio observatory dedicated to monitoring of AGN variability at 230 GHz. As a realistic example we use the Seoul National University Radio Observatory (SRAO) located in Seoul, Korea, at the geographic position 37°27′15″ N, 126°57′19″ E (Koo et al. 2003; Y.-S. Park, *priv. comm.*).

2. ANALYSIS

Our analysis progresses in three steps. Firstly, we estimate the signal-to-noise ratios (SNR) achievable by an SRAO-type observatory. Secondly, we select potential target sources based on AGN properties known from the literature. Thirdly, we provide a statistical analysis of various types of AGN variability and the corresponding detection limits. Given the angular resolution of a 6-m radio telescope, we can safely treat all our targets as point sources. Unless stated otherwise, all noise values refer to Gaussian 1σ levels.

2.1 Noise Limits

The *signal-to-noise ratio* achieved by a radio observatory can be calculated as follows:

$$\mathrm{SNR} = \frac{\mathrm{Signal}}{\mathrm{Noise}} = \frac{T_\mathrm{E}}{\delta T} = \frac{T_\mathrm{E}\sqrt{\Delta\nu\Delta t}}{T_\mathrm{sys}} \qquad (1)$$

where T_E is the equivalent temperature of the source, δT is the noise temperature of the telescope, $\Delta\nu$ is the observing bandwidth of the receiver, Δt is the integration time, and T_sys is the system temperature (cf. Wilson et al. 2008). All temperatures are in units of Kelvin. For a point source, the *equivalent temperature* T_E of the source is simply given by (Thompson et al. 2004)

$$T_\mathrm{E} = \frac{A_\mathrm{e}}{2k}F_\nu = \frac{A_\mathrm{e}}{2800}F_\nu \equiv F_\nu/\rho_A \qquad (2)$$

where k is Boltzmann's constant, and F_ν is the flux density of the source in units of Jansky (Jy); the conversion factor ρ_A (in units of Jy K^{-1}) is usually referred to as *antenna efficiency*. The effective light collecting area A_e is given by

$$A_\mathrm{e} = A_0\, e^{-(4\pi\zeta/\lambda)^2} \qquad (3)$$

where A_0 is the physical aperture area, ζ is the root-mean-squared difference between actual and ideal antenna surface, and λ is the observing wavelength. For the SRAO with an aperture of 6 m, $A_\mathrm{e}/A_0 \approx 0.55$ and $\rho_A = 180$ Jy K^{-1} at 230 GHz. The effective aperture is derived from holographic mapping of the antenna surface (Koo et al. 2003).

The crucial parameter for our analysis is the *system temperature* T_sys which can be written as

$$T_\mathrm{sys} = T_\mathrm{rec} + T_\mathrm{atm}\eta\left(1 - e^{-\tau_0 X(\theta)}\right) + T_\mathrm{amb}\,(1-\eta) \qquad (4)$$

where T_rec is the receiver noise temperature, T_atm is the atmosphere temperature, τ_0 is the optical depth of the atmosphere in zenith direction, $X(\theta)$ is the air mass at zenith angle θ, T_amb is the ambient temperature, and η is the spillover efficiency including rear spillover, scattering, blockage, and ohmic loss efficiency. In the present work we use the approximation $X(\theta) \approx \sec(\theta)$ as we consider only sources with $\theta \lesssim 60°$.

In order to arrive at quantitative signal-to-noise ratios, we make the following choices for the values of the various parameters. We assume $\eta = 0.9$, in agreement with typical values for modern receivers. For the receiver temperature we assume $T_\mathrm{rec} = 55$ K; this is five times the quantum noise limit given by $h\nu/k \approx 11$ K and typical for modern receivers (cf. Eq. 5.20 of Wilson et al. 2008; h denotes Planck's constant). In agreement with typical winter conditions at the SRAO site, the remaining temperature terms are assumed to be $T_\mathrm{atm} = 263$ K and $T_\mathrm{amb} = 273$ K, with a – rather conservative – atmospheric optical depth of $\tau_0 = 1.5$; to take into account an average air mass, we use $\theta = 45°$. Additionally, we assume a bandwidth of $\Delta\nu = 1$ GHz and select an integration time of $\Delta t = 100$ s. Accordingly, we find $T_\mathrm{sys} = 290$ K and $\delta T = 0.9$ mK, corresponding to a noise level in units of flux density of $\sigma_N = 0.16$ Jy. All parameters, as well as the resulting noise values, are summarized in Table 1.

Table 2.
Candidate target sources for an SRAO-type radio observatory with SNR≥10

ID (B1950)	Redshift	R.A.	DEC	F_ν	ν_0	SNR	Type
0059+581[e,f]	0.644	01h02m45.7s	58d24m11s	1.9	230	12	LPQ
0133+476[a]	0.85	01h36m58.6s	48d51m29s	1.7	94	11	HPQ/Blazar/FSRQ
0235+164[a,b,f]	0.94	02h38m38.9s	16d36m59s	2.1	230	13	FSRQ/BLLac
0300+470	0.47	03h03m35.2s	47d16m16s	1.7	86	11	BLLac
0316+413	0.017	03h19m48.1s	41d30m42s	4.8	230	32	Sy2/NLRG
0355+508	1.52	03h59m29.7s	50d57m05s	4.2	230	27	LPQ
0415+379	0.048	04h18m21.3s	38d01m36s	4.5	230	30	Sy1/BLRG
0420−014	0.91	04h23m15.8s	−01d20m33s	2.5	231	16	Blazar/BLLac/HPQ
0432+052	0.03	04h33m11.1s	05d21m16s	1.6	230	10	LPQ/BLRG
0528+134	2.07	05h30m56.4s	13d31m55s	2	230	13	LPQ/FSRQ/Blazar
0607−157[c]	0.32	06h09m40.9s	−15d42m41s	2.4	110	14	FSRQ
0727−115	1.59	07h30m19.1s	−11d41m13s	2.3	100	13	RLQ
0748+126	0.88	07h50m52.0s	12d31m05s	2.3	230	14	LPQ/FSRQ
0827+243	0.94	08h30m52.1s	24d11m00s	1.6	96	10	FSRQ/LPQ/Blazar
0851+202	0.3	08h54m48.9s	20d06m31s	4	230	26	BLLac
0923+392	0.69	09h27m03.0s	39d02m21s	2.6	230	17	Sy1/LPQ
1030+415	1.11	10h33m03.7s	41d16m06s	1.5	94	10	HPQ/FSRQ
1055+018	0.89	10h58m29.6s	01d33m59s	2.5	230	15	HPQ/BLLac
1253−055	0.53	12h56m11.1s	−05d47m22s	9.5	230	58	BLLac/HPQ/FSRQ
1334−127	0.53	13h37m39.8s	−12h57m25s	3.8	230	22	HPQ/BLLac
1510−089	0.36	15h12m50.5s	−09d06m00s	1.6	230	10	Sy1/HQP
1606+106	1.22	16h08m46.2s	10d29m08s	1.8	94	11	FSRQ/LPQ/Blazar
1633+382	1.81	16h35m15.5s	38d08m04s	1.8	230	12	FSRQ/LPQ/Blazar
1641+399	0.592	16h42m58.8s	39d48m37s	2.8	230	18	HPQ/FSRQ
1642+690[a,b,f]	0.75	16h42m07.8s	68d56m40s	2.3	230	14	HPQ/FSRQ
1730−130	0.902	17h23m02.7s	−13d04m50s	2.4	230	14	BLLac/FSRQ/LPQ
1749+096	0.322	17h51m32.8s	09d39m01s	2.7	230	17	HPQ/BLLac
2013+370	—	20h15m28.7s	37d11m00s	2.2	230	14	BLLac
J2044−1043	0.034	20h44m09.7s	−10d43m25s	2.1	190	12	Sy1.2
2145+067	0.99	21h48m05.4s	06d57m39s	1.6	230	10	LPQ/FSRQ
2200+420[d]	0.068	22h02m43.3s	42d16m40s	1.8	230	12	BLLac
2216−038	0.901	22h18m52.0s	−03h35m37s	1.6	262	10	FSRQ/LPQ
2223−052	1.4	22h25m47.2s	−04d57m01s	2.4	230	14	HPQ/BLLac

NOTES: F_ν is the source flux at 230GHz in units of Jy, ν_0 is the observation frequency of data taken from the NED, in units of GHz. Entries "—" denote "not available". For some objects IDV has been reported by the studies referred to below.

REFERENCES: a — Quirrenbach et al. 1992; b — Quirrenbach et al. 2000; c — Kedziora-Chudczer et al. 2001; d — Kraus et al. 2003; e — Lovell et al. 2003; f — Ojha et al. 2004

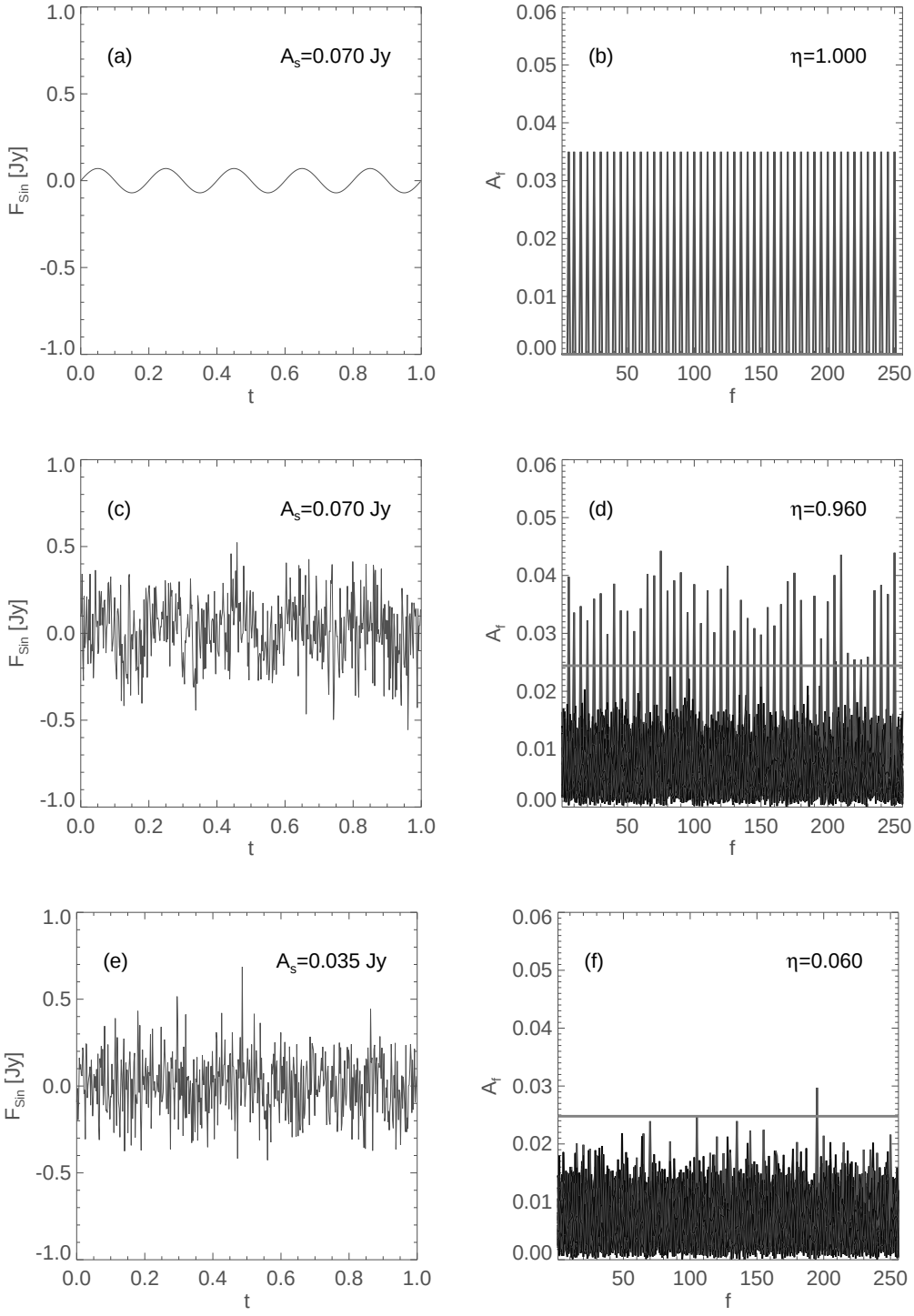

Fig. 1.— Illustration of the analysis scheme for PERIODIC VARIABILITY. **a.** Idealized, noise-free variable lightcurve with amplitude $A_s = 0.07$ Jy and variability frequency $f = 5$. **b.** Overlay of 50 Fourier transforms of noise-free lightcurves with $A_s = 0.07$ Jy and $f = 5, 10, ..., 250$; as the signals are free of noise, the detection efficiency η is unity. **c.** Like **a** but with Gaussian noise with amplitude $\sigma_N = 0.16$ Jy. **d.** Like **b** but for lightcurves with noise σ_N. The horizontal grey line marks the 5σ detection threshold. **e.** Like **c** but with variability amplitude reduced to $A_s = 0.035$ Jy. **f.** Like **d** but for lightcurves with $A_s = 0.035$ Jy. The substantial decrease in detection efficiency between **d** and **f** is obvious.

2.2 Source Selection

In order to select a set of candidate target sources, we first extracted a list of 407 radio-bright AGN from the NASA/IPAC Extragalactic Database (NED). Unfortunately, the data taken at 230GHz is unavailable for all sources. In such cases, we obtained reference fluxes F_{ν_0}, where ν_0 is a frequency as close to 230 GHz as possible. We made the usual assumption that the radio spectra of our target AGN follow a power law

$$F_\nu = F_{\nu_0} \left(\frac{\nu}{\nu_0}\right)^{-\alpha} \tag{5}$$

where F_ν is the source flux at frequency ν, F_{ν_0} is the source flux at frequency ν_0, and α is the spectral index. We assumed a typical spectral index $\alpha = 0.6$ to estimate the source fluxes at 230 GHz.

We aim at target sources with SNR sufficient to detect rapid variability. Accordingly, our final sample is composed of sources with (1) signal-to-noise ratios larger than or equal to ten, and (2) transit zenith angles less than 60°. For each source we computed an individual σ_N using the zenith angle at transit for reference and from this the corresponding signal-to-noise ratio. For the location of the SRAO, this left us with 33 sources. The source with the highest SNR turned out to be 1253−055 ($F_{230\,\mathrm{GHz}} \approx 9.5$ Jy, SNR≈58), the source with the lowest SNR was 1030+415 ($F_{230\,\mathrm{GHz}} \approx 1.5$Jy, SNR≈10). We summarize our sample in Table 2; we note that for five of our target AGN intra-day variability has already been reported in the literature.

We employed various checks to ensure the reliability of our sample. Modifying the values for various critical parameters, especially α, changes the number of selected targets by less than 20%. Therefore we conclude that our sample is fairly insensitive to the choice of parameters.

2.3 Detection Limits of Variability

Our study also aims at a quantitative description of the variability that might be detected under the conditions outlined above. Accordingly, we analyze simulated, though realistic, observations statistically by means of Monte Carlo simulations. In the following, we always assume a single long – $\mathcal{T}$=14.2 h – observation of an arbitrary target. The observation time is divided into 512 bins of 100 s each. Our calculations address two types of potential variability: a periodic flux modulation (periodic variability) and a single outburst of activity (flaring variability). Calculations are performed in IDL.*

2.3.1 Periodic Variability

An artificial lightcurve corresponding to a noisy signal with periodic variability and zero average, $F_{\sin}$, is created by

$$F_{\sin} = A_{\mathrm{s}}\ \sin(2\pi f t) + F_{\mathrm{noise}} \tag{6}$$

where A_{s} is the amplitude of the modulation, f is the frequency of the periodic modulation, $0 \le t \le 1$ is the time in units of the total observing time $\mathcal{T}$, and F_{noise} is Gaussian random noise with amplitude σ_N.

We analyze any simulated lightcurve by taking the absolute value of its Fourier transform. We classify flux variability as detected if the Fourier transform has a peak exceeding its average by five times its standard deviation.† In order to derive detection thresholds, we examine 50 different amplitudes $A_{\mathrm{s}} = 0.005, 0.01, ..., 0.25$ Jy. For each amplitude, we probe 50 different frequencies $f = 5, 10, ..., 250$.‡ For a given amplitude A_s, we define a *detection efficiency*

$$\eta_{\mathrm{P}}(A_{\mathrm{s}}) = \frac{N_{\mathrm{d,P}}}{50} \tag{7}$$

where $N_{\mathrm{d,P}}$ is the number of detections which is 50 at best (for 50 frequencies of periodic variability). In or-

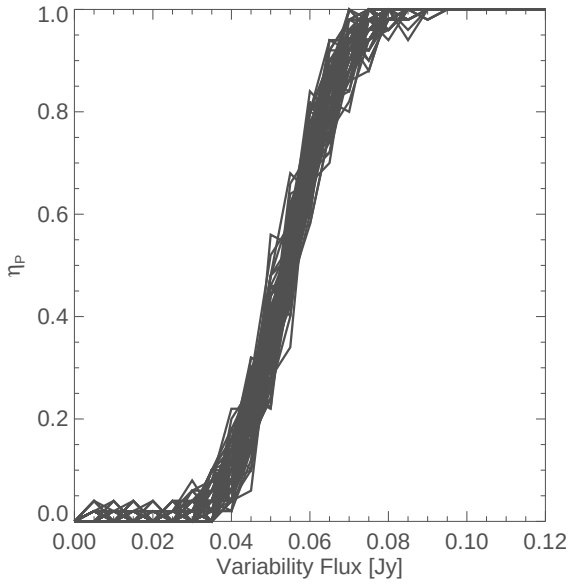

Fig. 2.— Detection efficiency η_P of PERIODIC VARIABILITY as function of amplitude of flux variation. This diagram is an overplot of 100 analysis runs (grey lines); for each flux amplitude, 100 values of η_P are computed, thus showing the confidence ranges.

*Interactive Data Language, ITT Exelis Inc., McLean (Virginia)

†This straightforward approach is possible because our artificial data are evenly sampled. Realistic flux observations usually require the use of periodograms for which the false alarm probability follows an exponential distribution (Scargle 1982).

‡As we normalize the total observing time to the range [0, 1], the frequencies are simply unit-free integers. The Nyquist frequency is half the number of data points, i.e. 256 in our case.

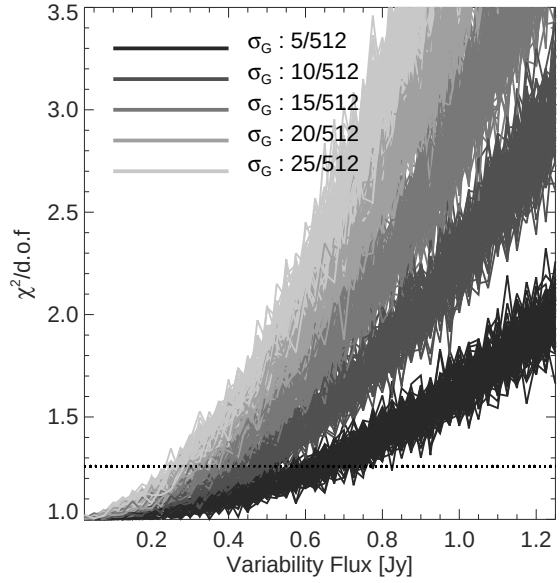

Fig. 3.— Reduced χ^2 test probing the detection of FLARING VARIABILITY. The reduced χ^2 is shown here as function of variability flux A_G, for five different flare time scales σ_G. For each σ_G, 100 curves – one for each realization – are plotted on top of each other. The horizontal dotted line marks the χ^2/d.o.f. = 1.26 limit above which significant variability is detected.

der to obtain statistically robust results, we test each combination of f and A_s 100 times, meaning we analyze 250,000 simulated lightcurves in total. We illustrate our analysis procedure in Fig. 1 and present the detection efficiency as function of amplitude in Fig. 2.

2.3.2 Flaring Variability

In order to create an artificial lightcurve with episodic, flaring variability, we parametrize the flare as a singular flux peak with Gaussian shape. Accordingly, our simulated time series is

$$F_{\rm Gauss} = A_{\rm G}\ \exp\left[-\frac{(t-0.5)^2}{2\sigma_{\rm G}^2}\right] + F_{\rm noise} \qquad (8)$$

where A_G is the flare amplitude, t is the time in units of total observing time, σ_G^2 is the temporal variance of the flux peak (variability time scale), and $F_{\rm noise}$ is Gaussian random noise with amplitude σ_N. The flare is centered at $t = 0.5$. This parametrization takes into account explicitly that the detectability of a flux peak depends on its amplitude as well as its time scale. We examine 50 different flare amplitudes $A_{\rm G}$ and five flare time scales $\sigma_{\rm G} = 5/512, 10/512, ..., 25/512$, i.e., 250 parameter combinations in total.

Reduced χ^2 Test: Apart from periodic variability, there is no obvious recipe for the detection of flaring flux modulations. A simple approach is provided by a χ^2 test that uses a signal constant in time (absence of variability) as null hypothesis. Taking into accounts the number of degrees of freedom leads to a *reduced* χ^2 test

$$\chi^2/{\rm d.o.f.} = \frac{1}{N-1}\sum_{i=1}^{N}\frac{F_{{\rm Gauss},i}^2}{\sigma_{\rm N}^2} \qquad (9)$$

where $F_{{\rm Gauss},i}$ is the i-th value of the lightcurve defined by Eq. 8, d.o.f. denotes the number of degrees of freedom, and N is the number of data points. In case of absence of variability, χ^2/d.o.f. ≈ 1 by construction. We calculate 100 realizations of χ^2/d.o.f. for each combination of A_G and σ_G, meaning 25,000 calculations in total. We examine a range of flare amplitudes $A_{\rm G} = 0.025, 0.05, ..., 1.25$ Jy. In Fig. 3 we show χ^2/d.o.f. as function of A_G for the five flare time scales examined. We consider the null hypothesis "the lightcurve is not variable" as rejected if χ^2/d.o.f. ≥ 1.26, corresponding to a Gaussian significance of 5σ for 511 degrees of freedom. With increasing flare duration, i.e., increasing number of data points affected, the minimum flare amplitude necessary for detection decreases.

Multi-Scale Analysis: A more sophisticated but straightforward approach to detecting flaring variability is provided by *multi-scale analysis* (e.g., Starck & Murtagh 2006). The underlying scheme is the following:

1. Take a simulated lightcurve and search for a signal in excess of five times the noise level of the data.
2. Bin the lightcurve such that $\mathcal{N}$ adjacent data points are combined into one averaged value.
3. Repeat step 1.

We apply this scheme to our data in an iterative fashion. In each binning level $n = 0, 1, 2, 3, 4, 5$ we combine two adjacent data points such that $\mathcal{N}$=2^n data points of the original lightcurve have been combined after step n; the case $n = 0$ simply corresponds to the original time series. Binning reduces the noise in a lightcurve from σ_N to $\sigma_N/\sqrt{\mathcal{N}}$. Using our usual 5σ criterion for counting a detection as significant, we are able to detect flux peaks with amplitudes $5\sigma_N/\sqrt{\mathcal{N}}$ – provided the flux peak actually covers approximately $\mathcal{N}$ data points in the original lightcurve. We illustrate our analysis scheme in Fig. 4.

We analyze 100 realizations for each combination of flare amplitude A_G, flare time scale σ_G, and binning level n, meaning 150,000 lightcurves in total. We examine a range of flare amplitudes $A_{\rm G} = 0.017, 0.034, ..., 0.85$ Jy. We define a detection efficiency

$$\eta_{\rm F}(A_{\rm G}, \sigma_{\rm G}, n) = N_{\rm d,F}/100 \qquad (10)$$

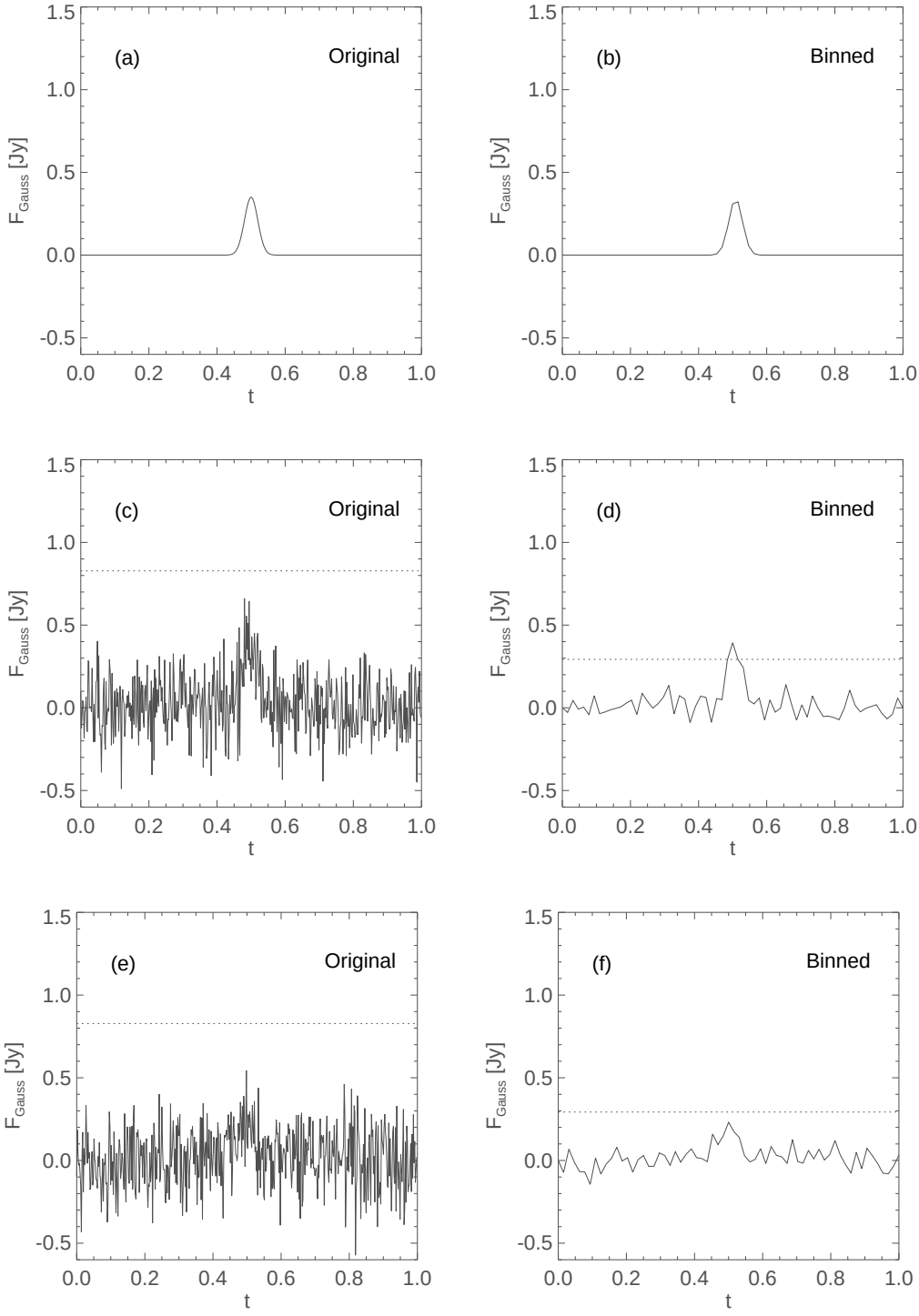

Fig. 4.— Illustration of the MULTI-SCALE ANALYSIS scheme for FLARING VARIABILITY. **a.** Idealized, noise-free lightcurve with a Gaussian flux peak with amplitude $A_G = 0.35\,\mathrm{Jy}$ and width $\sigma_G = 20/512$. **b.** The lightcurve **a** with $\mathcal{N}$=8 adjacent data points being binned into one. **c.** Lightcurve **a** with Gaussian noise with amplitude $\sigma_N = 0.16\,\mathrm{Jy}$ added. **d.** Binned version of lightcurve **c**. **e.** Like lightcurve **c** but with flux peak amplitude reduced to $A_G = 0.17\,\mathrm{Jy}$. **f.** Binned version of **e**. In all diagrams the horizontal dotted lines mark the respective 5σ detection thresholds. The impact of binning and flux peak amplitude is obvious.

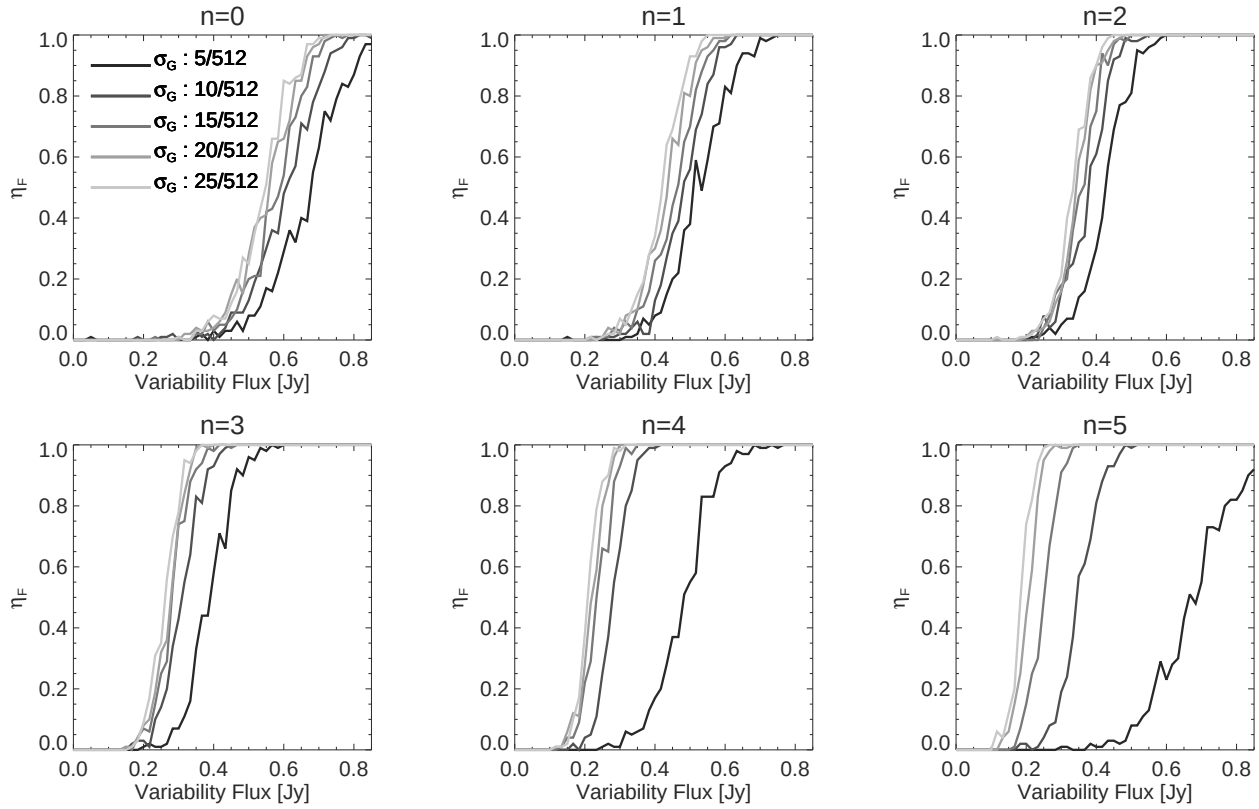

Fig. 5.— Detection efficiency η_F for FLARING VARIABILITY as function of flux peak amplitude (variability flux) and binning level n derived from MULTI-SCALE ANALYSIS. Each diagram shows five curves corresponding to the five flare time scales indicated in the top left panel.

where $N_{\rm d,F}$ is the number of times variability is detected out of 100 trials for a given set of A_G, σ_G, and n. The resulting detection efficiencies are shown in Fig. 5.

3. DISCUSSION

Our analysis probes the capabilities of a 6-meter class radio telescope with respect to continuum flux observations of AGN intra-day variability at high radio frequencies around 230 GHz. Assuming typical weather conditions for the location of the SRAO and the validity of the usual noise laws of radio astronomy, we conclude that an SRAO-type observatory is affected by a statistical (1σ) noise limit of $\sigma_N \approx 0.16$ Jy. Demanding a signal-to-noise ratio ≥ 10 for AGN flux monitoring, we are able to identify 33 sources observable from the location of the SRAO (Table 2). Thus we may conclude that an SRAO-type observatory is indeed able to make valuable contributions to monitoring studies of AGN.

We note that our calculations throughout Section 2 assume somewhat idealized observations leading to densely sampled lightcurves without interruptions. In realistic observations, the need for occasional calibrations of flux and amplitude, the observing schemes, and technical boundary conditions will result in more complicated datasets with details depending on the characteristics of the observatory actually employed. Our results depend only weakly on our choice for the total observing time $\mathcal{T}$=14.2 h: shorter observing times reduce the maximum time scale of observable flux variations, but not the sensitivity (which is calculated for 100 s of integration time).

Unsurprisingly, the limit for the detection of flux variations depends on the morphology of the variability. We analyze two rather extreme examples, namely periodic and flaring flux modulations. The detection efficiency (Figs. 1, 2) of *periodic* variability – which takes into account many different frequencies of modulation up to almost the Nyquist limit – approaches unity when the amplitude of flux modulations exceeds approximately 0.08 Jy. The detection limits for *flaring* variability show a strong interplay between the amplitude of a flux peak and its duration: shorter flares require larger amplitudes in order to be detected. A simple χ^2 test (Fig. 3) indicates that the minimum amplitudes necessary are approximately located between 0.3 Jy and 0.8 Jy for characteristic flare time scales σ_G between 25/512 (in units of total observing time,

corresponding to ≈42 min) and 5/512 (≈8 min). Using a more sophisticated multi-scale analysis and demanding detection efficiencies close to unity (Figs. 4, 5) reduces these limits to the range from ≈0.3 Jy to ≈0.5 Jy. In realistic AGN lightcurves, variability follows red noise power laws (e.g., Trippe et al. 2011; Park & Trippe 2012) with stronger flux modulations occurring on longer time scales; red noise variability may be regarded as a case intermediate between periodic and flaring variability. Notably, we may conclude from our analyses that we are able to detect significant variability with amplitudes $\lesssim 2\sigma_N \approx 0.3$ Jy, i.e., on levels $\lesssim 10\%$ of the average fluxes of our targets.

The physical conditions within a target AGN can be probed via analysis of timescales and amplitudes of flux variations. Using realistic astrophysical parameter values, the observed brightness temperature can be expressed (Wagner & Witzel 1995) as

$$T_{\rm b} = 4.5 \times 10^{10}\, A_{\rm var} \left[\frac{\lambda\, d}{t_{\rm var}(1+z)}\right]^2 \ {\rm K} \qquad (11)$$

where $A_{\rm var}$ is the amplitude of a flux modulation (in units of Jy), λ is the wavelength (in cm), d is the distance to the source (in Mpc), $t_{\rm var}$ is the variability timescale (in days), and z is the redshift of the source. For a source at $z = 0.3$ with $A_{\rm var} = 0.3$ Jy and $t_{\rm var} = 40$ min, $T_b \approx 10^{17}$ K for observations at 230 GHz. Even for variability timescales on the order of one day, $T_b \approx 10^{14}$ K. Accordingly, any detection of intra-day variability with an SRAO-type radio observatory corresponds to the observations of sources with observed brightness temperatures exceeding the Inverse-Compton limit. Using the common assumption that such an excess in observed brightness temperature is due to Doppler boosting in AGN outflows (e.g., Fuhrmann et al. 2008) one finds an expression for the Doppler factor δ as

$$\delta = (1+z)\left(\frac{T_b}{10^{12}\,{\rm K}}\right)^{1/(3-\alpha)} \qquad (12)$$

where z is the redshift of the source and α is the spectral index (cf. Eq. 5). For observed $T_b \approx 10^{14-17}$ K, $\delta \approx$ 8–150 – meaning that we are, a priori, able to probe a wide range of plasma-physical and kinematic conditions within AGN.

High-frequency radio monitoring of radio-bright compact AGN is an important complement to simultaneous observations at other wavelengths, both for single-dish flux monitoring (e.g., Fuhrmann et al. 2008) as well as radio-interferometric mapping (e.g., Lee et al. 2008). An important example is the measurement of time lags between lightcurves obtained at different frequencies, providing the dispersion measure – the line-of-sight integral of the particle density – and thus information on the matter content of the emission region (e.g., Wilson et al. 2008). Accordingly, the combination of small, 6-m class observatories working at high frequencies with larger observatories working at lower frequencies – like the Korean VLBI Network (KVN) which operates at frequencies of 22, 43, 86, and 129 GHz (Kim et al. 2011; Lee et al. 2011) – is likely to provide new insights into AGN physics.

4. CONCLUSIONS

In this article, we study the feasibility of high-frequency radio observations of AGN intra-day variability. We assume the use of a small 6-meter class observatory for continuum flux monitoring at 230 GHz, using the SNU Radio Astronomical Observatory (SRAO) as a realistic example. Our work arrives at the following principal conclusions:

1. Assuming an integration time of 100 s per flux measurement, a spectral bandwidth of 1 GHz, and typical SRAO winter conditions, the statistical 1σ noise limit is $\sigma_N \approx 0.16$ Jy.
2. Demanding a signal-to-noise ratio ≥ 10, we compile a list of 33 radio-bright compact AGN with fluxes $F_\nu \gtrsim 1.5$ Jy that are observable at the geographic location of the SRAO.
3. Based on results from exhaustive Monte-Carlo simulations, we conclude that it is possible to detect significant (referring to a 5σ detection threshold) variability with amplitudes $\lesssim 0.3$ Jy, roughly 10% of the typical fluxes of our candidate target sources. Details depend on the morphology of variability – periodic, episodic/flaring, or intermediate.
4. For nearby AGN (using here $z = 0.3$ for reference), observable flux modulations correspond to observed brightness temperatures $T_b \approx 10^{14-17}$ K, meaning Doppler factors of $\delta \approx$ 8–150. This indicates that observations of the type we study are able to probe a wide range of plasma-physical and kinematic conditions within AGN.

Overall, we are able to conclude that high-frequency radio observations of AGN intra-day variability with dedicated small observatories can provide valuable new insights into AGN physics. This approach is especially powerful when combining those high-frequency radio observations with data from other facilities like the KVN.

ACKNOWLEDGMENTS

We are grateful to Yong-Sun Park for enlightening discussion and to Junghwan Oh (both at SNU) for valuable technical support. We acknowledge financial support from the Korean Astronomy and Space Science Institute (KASI) via Research Cooperation Grant 2012-1-600-90. Our work has made use of the NASA/IPAC Extragalactic Database (NED) which is operated by the Jet Propulsion Laboratory, California Institute of Technology, under contract with the

National Aeronautics and Space Administration of the USA. Last but not least, we are greatful to an anonymous reviewer whose careful report helped to improve this paper.

REFERENCES

Beckmann, V., & Shrader, C. 2012, Active Galactic Nuclei (Weinheim: Wiley-VCH)

Blandford, R. D., & Königl, A. 1979, Relativistic Jets as Compact Radio Sources, ApJ, 232, 34

Fuhrmann, L., et al. 2008, Testing the Inverse-Compton Catastrophe Scenario in the Intra-Day Variable Blazar S5 0716+71. III. Rapid and Correlated Flux Density Variability from Radio to Sub-mm Bands, A&A, 490, 1019

Gabanyi, K. E., et al. 2007, The IDV Source J1128+5925, a New Candidate for Annual Modulation?, A&A, 470, 83

Kedziora-Chudczer, L. L., Jauncey, D. L., Wieringa, M. H., Tzioumis, A. K., & Reynolds, J. E. 2001, The ATCA Intraday Variability Survey of Extragalactic Radio Sources, MNRAS, 325, 1411

Kellermann, K. I., & Pauliny-Toth, I. I. K. 1969, The Spectra of Opaque Radio Sources, ApJ, 155, L71

Kim, K.-T., et al. 2011, 100-GHz Band Test Observations of the KVN 21-m Radio Telescopes, JKAS, 44, 81

Koo, B.-C., Park, Y.-S., Hong, S. S., et al. 2003, Performance of the SRAO 6-meter Radio Telescope, JKAS, 36, 43

Kraus, A., Krichbaum, T. P., Wegner, R., et al. 2003, Intraday Variability in Compact Extragalactic Radio Sources. II. Observations with the Effelsberg 100m Radio Telescope, A&A, 401, 161

Lee, S.-S., et al. 2008, A Global 86 GHz VLBI Survey of Compact Radio Sources, AJ, 136, 159

Lee, S.-S., et al. 2001, Single-Dish Performance of KVN 21 m Radio Telescopes: Simultaneous Observations at 22 and 43 GHz, PASP, 123, 1398

Liu, X., Song, H.-G., Marchili, N., Liu, B.-R., Liu, J., Krichbaum, T. P., Fuhrmann, L., & Zensus, J. A. 2012, Intra-Day Variability Observations of S5 0716+714 over 4.5 Years at 4.8 GHz, A&A, 543, A78

Lovell, J. E. J., Jauncey, D. L., Bignall, H. E., Kedziora-Chudczer, L., Macquart, J.-P., Rickett, B. J., & Tzioumis, A. K. 2003, First Results from MASIV: The Microarcsecond Scintillation-induced Variability Survey, AJ, 126, 1699

Lovell, J. E. J., Rickett, B. J., Macquart, J.-P., et al. 2008, The Micro-Arcsecond Scintillation-Induced Variability (MASIV) Survey. II. The First Four Epochs, ApJ, 689, 108

Marchili, N., et al. 2012, A Seasonal Cycle and an Abrupt Change in the Variability Characteristics of the Intraday Variable Source S4 0954+65, A&A, 542, A121

Ojha, R., Fey, A. L., Jauncey, D. L., Lovell, J. E. J., & Johnston, K. J. 2004, Milliarcsecond Structure of Microarcsecond Sources: Comparison of Scintillating and Nonscintillating Extragalactic Radio Sources, ApJ, 614, 607

Park, J.-H., & Trippe, S. 2012, Multiple Emission States in Active Galactic Nuclei, JKAS, 45, 147

Quirrenbach, A., et al. 1992, Statistics of Intraday Variability in Extragalactic Radio Sources, A&A, 258, 279

Quirrenbach, A., et al. 2000, Intraday Variability in Compact Extragalactic Radio Sources. I. VLA Observations, A&AS, 141, 221

Rickett, B. J., Coles, W. A., & Bourgois, G. 1984, Slow Scintillation in the Interstellar Medium, A&A, 134, 390

Scargle, J. D. 1982, Studies in Astronomical Time Series Analysis. II - Statistical Aspects of Spectral Analysis of Unevenly Spaced Data, ApJ, 263, 835

Starck, J.-L., & Murtagh, F. 2006, Astronomical Image and Data Analysis, 2nd edn. (Berlin: Springer)

Thompson, A. R., Moran, J. M., & Swenson, G. W. 2004, Interferometry and Synthesis in Radio Astronomy (Weinheim: Wiley-VCH)

Trippe, S., et al. 2011, The Long-Term Millimeter Activity of Active Galactic Nuclei, A&A, 533, A97

Wagner, S. J., & Witzel, A. 1995, Intraday Variability in Quasars and BL Lac Objects, ARA&A, 33, 163

Wilson, T. L., Rohlfs, K., & Hüttemeister, S. 2008, Tools of Radio Astronomy (Berlin: Springer)

Witzel, A., Heeschen, D. S., Schalinski, C., & Krichbaum, T. P. 1986, Kurzzeit-Variabilität Extragalaktischer Radioquellen, Mitt. Astron. Ges., 65, 239